



Cite this: DOI: 10.1039/c8tb02772b

## Zwitterionic shielded polymeric prodrug with folate-targeting and pH responsiveness for drug delivery†

Lei Li,<sup>a</sup> Yue Song,<sup>a</sup> Jinlin He,<sup>a</sup> <sup>a</sup> Mingzu Zhang,<sup>a</sup> Jian Liu <sup>b</sup> and Peihong Ni <sup>\*a</sup>

Zwitterionic polymers are a class of polymers that acts as both Lewis base and Lewis acid in solution. These polymers not only have excellent properties of hydration, anti-bacterial adhesion, charge reversal and easy chemical modification, but also have characteristics of long-term circulation and suppress nonspecific protein adsorption *in vivo*. Here, we describe a novel folate-targeted and acid-labile polymeric prodrug under the microenvironment of tumor cells, abbreviated as FA-P(MPC-co-PEGMA-BZ)-g-DOX, which was synthesized *via* a combination of reversible addition–fragmentation chain transfer (RAFT) copolymerization, Schiff-base reaction, Click chemistry, and a reaction between the amine group of doxorubicin (DOX) and aldehyde functionalities of P(MPC-co-PEGMA-BZ) pendants, wherein MPC and PEGMA-BZ represent 2-(methacryloyloxy)ethyl phosphorylcholine and polyethylene glycol methacrylate ester benzaldehyde, respectively. The polymeric prodrug could self-assemble into nanoparticles in an aqueous solution. The average particle size and morphologies of the prodrug nanoparticles were observed by dynamic light scattering (DLS) and transmission electron microscopy (TEM), respectively. We also investigated the *in vitro* drug release behavior and observed rapid prodrug nanoparticle dissociation and drug release under a mildly acidic microenvironment. The methyl thiazolyl tetrazolium (MTT) assay verified that the P(MPC-co-PEGMA-BZ) copolymer possessed good biocompatibility and the FA-P(MPC-co-PEGMA-BZ)-g-DOX prodrug nanoparticles showed higher cellular uptake than those prodrug nanoparticles without the FA moiety. The results of cytotoxicity and the intracellular uptake of non-folate/folate targeted prodrug nanoparticles further confirmed that FA-P(MPC-co-PEGMA-BZ)-g-DOX could be efficiently accumulated and rapidly internalized by HeLa cells due to the strong interaction between multivalent phosphorylcholine (PC) groups and cell membranes. This kind of multifunctional FA-P(MPC-co-PEGMA-BZ)-g-DOX prodrug nanoparticle with combined target-ability and pH responsiveness demonstrates promising potential for cancer chemotherapy.

Received 21st October 2018,  
Accepted 17th December 2018

DOI: 10.1039/c8tb02772b

rsc.li/materials-b

<sup>a</sup> College of Chemistry, Chemical Engineering and Materials Science, State and Local Joint Engineering Laboratory for Novel Functional Polymeric Materials, Jiangsu Key Laboratory of Advanced Functional Polymer Design and Application, Suzhou Key Laboratory of Macromolecular Design and Precision Synthesis, Soochow University, Suzhou 215123, P. R. China. E-mail: phni@suda.edu.cn; Tel: +86-512-65882047

<sup>b</sup> Institute of Functional Nano and Soft Materials (FUNSOM), Soochow University, Suzhou, 215123, P. R. China

† Electronic supplementary information (ESI) available: Experimental details and characterization data. <sup>1</sup>H NMR and <sup>13</sup>C NMR spectra of PEGMA-BZ monomer. <sup>1</sup>H NMR spectra of 4-cyano-4-ethylsulfanylthiocarbonylsulfanylentanoic acid (CEP) and folic acid. <sup>31</sup>P spectrum of P(MPC-co-PEGMA-BZ) copolymer. UV-vis spectra of (A) P(MPC-co-PEGMA-BZ)-g-DOX prodrug, (B) P(MPC-co-PEGMA-BZ), and (C) the reaction product of P(MPC-co-PEGMA-BZ) with triethylamine. UV-vis spectra of free folate and FA-P(MPC-co-PEGMA-BZ)-g-DOX in ethanol. Intensity ratios (*I*<sub>3</sub>/*I*<sub>1</sub>) as a function of Log C for (A) PMPD1 and (B) FA-PMPD1 prodrug nanoparticles in pH 7.4 buffer solution. TEM image of the PMPD1 prodrug nanoparticles (A) and the particle size distribution curve (B) corresponding to the TEM sample (scale bar 200 nm). Variation of particle size for the FA-PMPD1 prodrug nanoparticles in PBS 7.4 at different times. See DOI: 10.1039/c8tb02772b

## Introduction

During the past decades, cancer has been one of the most life-threatening diseases in the world.<sup>1</sup> The improvement of chemotherapy drugs on the aspects of their short half-time and severe toxicity to normal tissues remains an unmet need for clinical applications.<sup>2,3</sup> To overcome these limitations, polymeric prodrug nanoparticles as an emerging tool for cancer chemotherapy have been utilized because they have characteristic properties of increasing drug bioavailability, prolonging circulation time, and promoting accumulation in the tumor site.<sup>4–6</sup> In these prodrugs, the structure of polymers plays an important role in the performance and therapeutic effects.

Zwitterionic polymers possess both cationic and anionic groups but still remain charge neutral as a whole,<sup>7</sup> thus forming a strongly associated hydration layer through electrostatic interactions on the surface of drug delivery vessels and effectively

suppressing non-specific protein adsorption and foreign body reactions.<sup>8,9</sup> A synthetic polymer, which was inspired by the phosphorylcholine (PC) headgroup of the bilayer cell membrane, has been used to prepare or modify drug delivery carriers.<sup>10–12</sup> Zwitterionic polymers can minimize the interaction between the carriers and the biological components during the circulation process.<sup>13,14</sup>

Based on this, a new strategy has been proposed for improving the cellular internalization efficiency and the inefficient intracellular drug release of the prodrug, that is, the cell-adhering zwitterionic polymers. For example, poly(2-methacryloyloxyethyl phosphorylcholine) (polyMPC),<sup>15,16</sup> poly(sulfobetaine methacrylate) (polySBMA),<sup>17</sup> and poly(carboxybetaine methacrylate) (polyCBMA)<sup>18,19</sup> have been reported. Among them, polyMPC especially exhibits additional promise when conjugated to therapeutic proteins and chemotherapeutics. In addition, polymeric scaffolds with a zwitterionic 2-methacryloyloxyethyl phosphorylcholine (MPC) group containing a phosphate anion and a trimethylammonium cation with an inner-salt structure have attracted more attention.<sup>20</sup> Hence, polyMPC can be used as a drug delivery carrier due to its zwitterionic character with considerable advantages such as extensive water solubility, biocompatibility, and rapid cellular internalization.<sup>21,22</sup> These polymers have been widely synthesized to mimic the cell membranes and are considered as stealthy materials.<sup>23,24</sup>

In addition, polyMPC based polymers as drug carriers have also been widely investigated with respect to the prolongation of the circulation time, which verified that zwitterionic copolymers' nanoparticles possess good protein resistance properties and accelerate blood clearance during the circulation process.<sup>25–27</sup> Yusa and Ishihara prepared a type of pH-responsive polyion complex (PIC) vesicles consisting of water-soluble zwitterionic PMPC block and cationic or anionic blocks, which could be collapsed under acidic conditions and the drug was efficiently released from the lysosomes to the cytoplasm.<sup>28</sup> Ji *et al.* synthesized a pH-responsive PMPC-*b*-P(MEMA-hydrazide-DOX) prodrug, which was stable in blood circulation, with efficient cellular uptake and rapid drug release in cancer cells.<sup>29</sup> Yu *et al.*<sup>30</sup> prepared a novel pH responsive polymer–drug conjugate system poly(2-(methacryloyloxy)ethyl choline phosphate)-*b*-poly(2-methoxy-2-oxoethyl methacrylate-hyd-doxorubicin) (PCP-*b*-PMEMA-hyd-DOX), and confirmed that PCP-*b*-PMEMA-hyd-DOX can be easily and rapidly internalized by various cancer cells. Gong *et al.* reported a series of amphiphilic random-copolymers comprising MPC, stearyl methacrylate (SMA) and trimethoxysilylpropyl methacrylate (TSMA). They found that the polymeric nanoparticles could be stable in the presence of the cell membrane mimetic random-copolymers.<sup>31</sup> Luo *et al.* developed a DOX-conjugated poly(L-lysine)-*block*-poly(methacryloyloxyethyl phosphorylcholine) PLL(CB/DOX)-*b*-PMPC prodrug with 4-carboxy benzaldehyde grafted, which could promote the micellar structural disintegration in the tumor acid environment, leading to an endosomal escape as well as a rapid drug release to inhibit the tumor proliferation.<sup>32</sup>

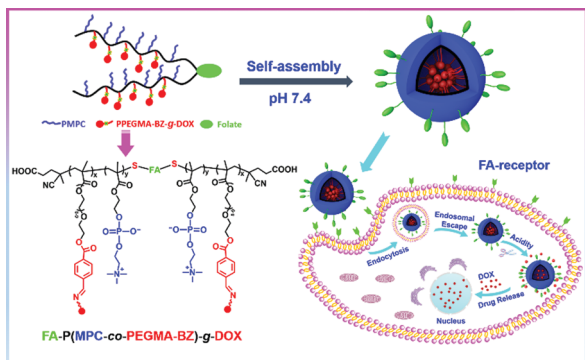
For enhancing the efficiency of the drug delivery and achieving rapid release at tumor sites, many researchers have conjugated

drugs onto the side chains of the polymers with acid-labile linkages, such as hydrazone,<sup>33,34</sup> acetal,<sup>35,36</sup> and imine,<sup>37–39</sup> whose cleavage enables the drug release in the tumor sites. It is well known that the typical pH of the normal cells is approximately 7.4, while the pH range can be as low as 5.0 to 6.0 in the endosomes of the cancer cells and much lower in the intracellular lysosomes (pH ~ 4.0–5.0) at the cellular level.<sup>40,41</sup> Cheng *et al.*<sup>42</sup> designed and prepared acid-sensitive polylactide-*graft*-doxorubicin (PLA-*g*-DOX) by azide–alkyne click reaction to transform acetylene functionalized PLA into PLA-*graft*-aldehyde (PLA-*g*-ALD), after which DOX was conjugated into the polymer scaffold by the Schiff base reaction, which can release DOX from PLA-*g*-DOX rapidly in an acidic medium due to the acid-labile Schiff base linkage between DOX and the polymer scaffold.

Prodrug nanoparticles can also enhance the accumulation of the drugs in the tumor site through the enhanced permeability and retention (EPR) effect.<sup>43</sup> For achieving good therapeutic efficacy, targeting ligands such as folic acid (FA),<sup>44,45</sup> biotin<sup>46,47</sup> and RGD<sup>48,49</sup> are introduced into the prodrug nanoparticles, which could be expected to reach the tumor site effectively *via* active targeting. Furthermore, folate receptors  $\alpha$  (FR $\alpha$ ) are most widely expressed at very low levels in normal tissues, but it is highly expressed in numerous cancers.<sup>50,51</sup> Folate-based drug delivery has been widely applied in tumor targeting for its high-affinity binding to the folate receptor, which also significantly decreases their toxic side effects compared to those of the non-targeted chemotherapy.<sup>52,53</sup>

In recent years, in the field of polymer synthesis, RAFT and click chemistry have been widely used. However, the folate-targeted polymeric prodrugs prepared through Schiff base reaction with a combination of RAFT and click chemistry methods have rarely been reported. It is important to develop neoteric and integrative tactics to enhance the stability, cellular internalization, intracellular drug release, and active targeting ability of the tumor cells simultaneously.

Herein, we first synthesized a new kind of zwitterionic random copolymer P(MPC-*co*-PEGMA-BZ) by RAFT copolymerization (Scheme 1). A pH-responsive polymeric prodrug was prepared using the amino group of DOX to react with the aldehyde groups of the P(MPC-*co*-PEGMA-BZ) pendants through a Schiff base reaction. Afterward, the thiol groups of P(MPC-*co*-PEGMA-BZ)-*g*-DOX were further reacted with the alkynyl groups of the propargyl folate by click chemistry. The polymeric prodrug could then self-assemble into nanoparticles in an aqueous solution, which could maintain the stability owing to the zwitterionic shell of the prodrug nanoparticles. Once the prodrug nanoparticles were internalized into the tumor site, they will easily bind to the cell membrane by means of the folate-receptor-mediated effect and rapidly internalize into the cell. The Schiff base bond (benzoic-imine) could be cleaved under the endosomal/lysosomal pH conditions. Then, the parent drug DOX could escape from the lysosome/endosome and diffuse into the cell nucleus, which could efficiently inhibit tumor cells proliferation. We provide a convenient method for the fabrication of the folate-targeted zwitterionic prodrug, and the resulting FA-P(MPC-*co*-PEGMA-BZ)-*g*-DOX prodrug nanoparticles have stability during circulation,

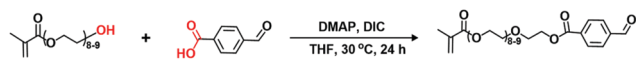


**Scheme 1** Illustration of zwitterionic shielded prodrug nanoparticles with folate-targeting for efficient intracellular release of hydrophobic anti-cancer drugs triggered by the acidic microenvironment inside the tumor tissue.

efficient cellular internalization and good targeting ability to tumor cells.

## Experimental section

### Preparation of polyethylene glycol methacrylate ester benzaldehyde (PEGMA-BZ) monomer



The synthesis procedure was carried out according to the reported methods with slight modifications.<sup>54</sup> Poly(ethylene glycol) methacrylate (0.02 mol, 10.0 g) and 4-carboxybenzaldehyde (0.04 mol, 6.0 g) were dissolved in anhydrous THF (120 mL) under nitrogen atmosphere. Afterward, the THF solution (30 mL) of *N,N'*-diisopropylcarbodiimide (DIC, 0.04 mol, 10.3 g) and 4-dimethylamino pyridine (DMAP, 0.01 mol, 1.22 g) was added dropwise at  $-5\text{ }^{\circ}\text{C}$ . The reaction mixture was heated to  $30\text{ }^{\circ}\text{C}$  for 48 h allowing the reaction to be completed. The solid deposited was filtered off and most of the THF was removed by a rotary evaporator. The crude product was further purified by silica gel column chromatography (10.5 g, yield: 83.1%).

### Synthesis of alkyne-functionalized folic acid (propargyl folate)

The synthesis of propargyl folate was accomplished by a method derived from the literature reports of folate conjugation.<sup>55</sup> Briefly, folic acid (1.0 g, 0.0022 mol) was dissolved in *N,N*-dimethylformamide (DMF, 10 mL) and cooled in an ice-water bath. *N*-Hydroxysuccinimide (260 mg, 0.0025 mol) and 1-(3-dimethylaminopropyl)-3-ethylcarbodiimide hydrochloride (EDC, 440 mg, 0.0025 mol) were added, and the resulting mixture was stirred in an ice-water bath for 30 min to give a white precipitate. A solution of propargylamine (124 mg, 2.25 mmol) with 5 mL of DMF was added, and the resulting mixture was stirred at  $25\text{ }^{\circ}\text{C}$  for 24 h. The reaction mixture was poured into water (100 mL) and stirred for 30 min to form a precipitate. The orange-yellow precipitate was filtered, washed with acetone, and dried under vacuum to a constant weight at  $30\text{ }^{\circ}\text{C}$  (0.8 g, yield: 71.2%).

### Synthesis of P(MPC-co-PEGMA-BZ) copolymer

The P(MPC-co-PEGMA-BZ) copolymer with pendant benzaldehyde groups was synthesized *via* RAFT polymerization. All magnetic stirring bars and glasswares used in the experiment were dried at  $120\text{ }^{\circ}\text{C}$  for 24 h and cooled under vacuum to eliminate the moisture before use. Briefly, MPC (1.12 g, 3.80 mmol), PEGMA-BZ (1.90 g, 3.04 mmol), CEP (10 mg, 0.038 mmol), and azobis(isobutyronitrile) (AIBN, 3.20 mg, 0.019 mol) were added into the flask together with a mixed solvent of 4 mL deionized water and 4 mL DMSO. After being degassed through three exhausting–refilling nitrogen cycles, the mixture was stirred under a nitrogen atmosphere at  $70\text{ }^{\circ}\text{C}$  for 12 h. Then, the flask was cooled to terminate the polymerization, and the raw product was subsequently dialyzed (MWCO 7000) against Milli-Q water for 24 h with the purpose of removing the unreacted monomers. The final product P(MPC-co-PEGMA-BZ) copolymer was obtained by lyophilization (2.3 g, yield: 76.0%).

### Synthesis of P(MPC-co-PEGMA-BZ)-g-DOX prodrug

P(MPC-co-PEGMA-BZ)-g-DOX prodrug was synthesized by Schiff base reaction. Briefly, P(MPC-co-PEGMA-BZ) (150 mg, 0.0025 mmol), DOX-HCl (80 mg, 0.147 mmol), and 0.5 mL of triethylamine (TEA) were dissolved in a mixture of deionized water (4 mL) and DMSO (4 mL), and subjected to ultrasound for 10 min. The mixture was stirred at  $30\text{ }^{\circ}\text{C}$  for 48 h. The raw product was subsequently dialyzed (MWCO 7000) against Milli-Q water with the purpose of removing the unreacted DOX. For forming the thiol-group of P(MPC-co-PEGMA-BZ)-g-DOX prodrug, we adjusted the dialysis water to an alkaline environment through the addition of a certain amount of TEA. The final product was obtained by lyophilization (180 mg, yield: 78.3%).

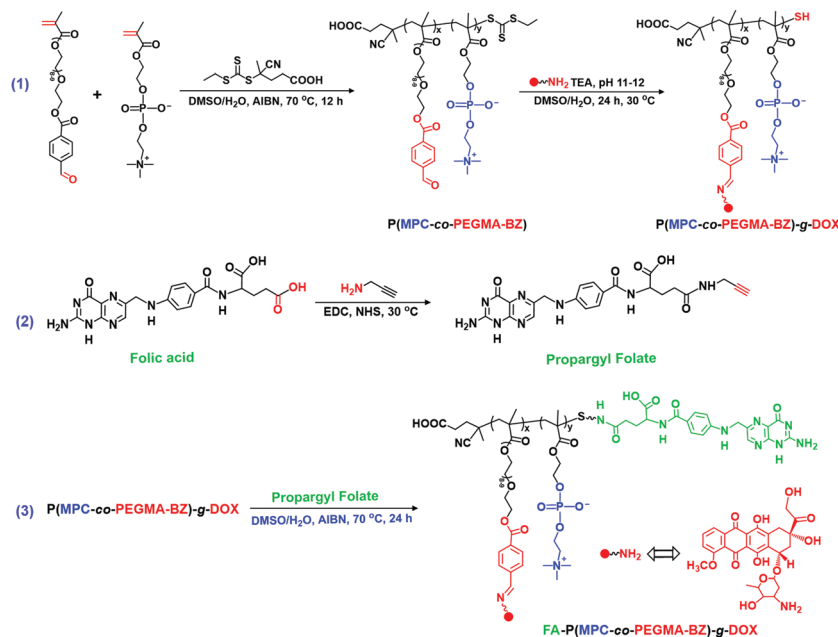
### Preparation of FA-P(MPC-co-PEGMA-BZ)-g-DOX prodrug by click chemistry

FA-P(MPC-co-PEGMA-BZ)-g-DOX prodrug was synthesized by click chemistry. All magnetic stirring bars and glasswares used in the experiment were dried at  $120\text{ }^{\circ}\text{C}$  for 24 h and cooled under vacuum to eliminate the moisture before use. Briefly, P(MPC-co-PEGMA-BZ)-g-DOX (100 mg, 0.0015 mmol), propargyl folate (7.37 mg, 0.015 mmol), and AIBN (5 mg, 0.030 mmol) were added into a flask together with 6 mL of deionized water/DMSO (v/v, 1/1). After being degassed through three exhausting–refilling nitrogen cycles, the mixture was stirred under a nitrogen atmosphere at  $70\text{ }^{\circ}\text{C}$  for 12 h. Then, the flask was cooled to terminate the polymerization, and the product was subsequently dialyzed (MWCO 7000) against Milli-Q water for 48 h; the dialysis water was adjusted to an alkaline environment. The final product was obtained by lyophilization (95.2 mg, yield: 88.7%).

## Results and discussion

### Synthesis and characterization of FA-P(MPC-co-PEGMA-BZ)-g-DOX prodrug

In this study, a novel acid-cleavable FA-P(MPC-co-PEGMA-BZ)-g-DOX prodrug was prepared through the combination of RAFT



Scheme 2 Synthesis routes of FA-P(MPC-co-PEGMA-BZ)-g-DOX polymeric prodrug.

copolymerization and click chemistry by the following steps, as shown in Scheme 2. First, the P(MPC-co-PEGMA-BZ) copolymer was synthesized by RAFT copolymerization of MPC and PEGMA-BZ monomers using 4-cyano-4-ethylsulfanylthiocarbonyl-sulfanylacetic acid (CEP) as chain transfer agent. Then, P(MPC-co-PEGMA-BZ)-g-DOX was synthesized by the Schiff base reaction. Finally, the targeting molecule, FA, was connected onto the terminal group of P(MPC-co-PEGMA-BZ)-g-DOX by click chemistry to yield the final product FA-P(MPC-co-PEGMA-BZ)-g-DOX.

The chemical structure of PEGMA-BZ monomer was verified by <sup>1</sup>H NMR and <sup>13</sup>C NMR analyses, which are shown in Fig. S1 and S2 in the ESI†. From these two figures, we identify three chemical shifts at δ 10.11 ppm (peak i), δ 8.23 ppm (peak g), and δ 7.97 ppm (peak h) that are all attributed to the protons of 4-carboxybenzaldehyde. Furthermore, the characteristic signals at δ 1.95 ppm, δ 3.65 ppm, δ 3.86 ppm, δ 4.30 ppm, δ 4.52 ppm, δ 5.58 ppm, and δ 6.13 ppm belong to the protons of -CO-C(CH<sub>2</sub>)-CH<sub>3</sub>, -CH<sub>2</sub>-CH<sub>2</sub>-OCO-, -CH<sub>2</sub>-CH<sub>2</sub>-OCO-, and -CO-C(CH<sub>2</sub>) of PEGMA-BZ monomer in Fig. S1 (ESI†), respectively. <sup>13</sup>C NMR (100 MHz, DMSO-d<sub>6</sub>, δ ppm): 191.55 (HCO-), 167.47 [CH<sub>3</sub>(CH<sub>2</sub>)-CO-O-], 165.32 (-OCO-CH<sub>2</sub>-), 125.81 [-CO-C-(CH<sub>2</sub>)-CH<sub>3</sub>], 70.67 (-CH<sub>2</sub>-CH<sub>2</sub>-O-CH<sub>2</sub>-CH<sub>2</sub>-), 64.68 (-CH<sub>2</sub>-CH<sub>2</sub>-O-CH<sub>2</sub>-CH<sub>2</sub>-), 18.54 [-C-(CH<sub>2</sub>)-CH<sub>3</sub>] (Fig. S2, ESI†). The chemical structure of CEP was characterized by <sup>1</sup>H NMR, as shown in Fig. S3 (ESI†). Afterward, a P(MPC-co-PEGMA-BZ) random copolymer was synthesized by RAFT copolymerization of MPC and PEGMA-BZ monomers using CEP as chain transfer agent, which was P(MPC<sub>45</sub>-co-PEGMA-BZ<sub>40</sub>). For the sake of simplicity, we designated the random copolymer as PMP1. As shown in Fig. 1, all the chemical shifts can be assigned to the protons of the PMP1 random copolymer. There are proton signals appearing at δ 10.01 ppm (peak i), δ 7.81–8.06 ppm (peak h + g), and δ 3.21 ppm (peak n) in Fig. 1, which can be attributed to the units of PEGMA-BZ and MPC in the PMP1 random copolymer.

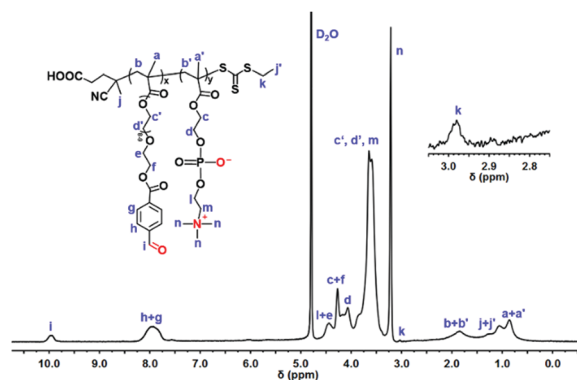


Fig. 1 <sup>1</sup>H NMR spectrum of PMP1 random copolymer.

We also characterized the chemical structure of PMP1 random copolymer by <sup>31</sup>P NMR, as shown in Fig. S4 (ESI†), which could further verify the successful synthesis of PMP1 random copolymer. The GPC trace of PMP1 random copolymer in Fig. 2 exhibited a unimodal peak with a polydispersity index of 1.62, and the  $\bar{M}_n$  value of PMP1 random copolymer is  $1.70 \times 10^4$  g mol<sup>-1</sup>. Then, the P(MPC-co-PEGMA-BZ)-g-DOX prodrug (abbreviated as PMPD1) was characterized by <sup>1</sup>H NMR spectroscopy. As shown in Fig. 3, some chemical shifts at δ 10.01 ppm and δ 7.81–8.06 ppm of the PMPD1 prodrug disappeared, indicating that the aldehyde group in the side chain of the P(MPC-co-PEGMA-BZ) copolymer completely reacted through the Schiff base reaction.

The polymerization degrees of P(MPC-co-PEGMA-BZ) were calculated according to the <sup>1</sup>H NMR analysis by the following eqn (1) and (2):

$$\frac{A_k}{A_n} = \frac{2}{9y} \quad (1)$$

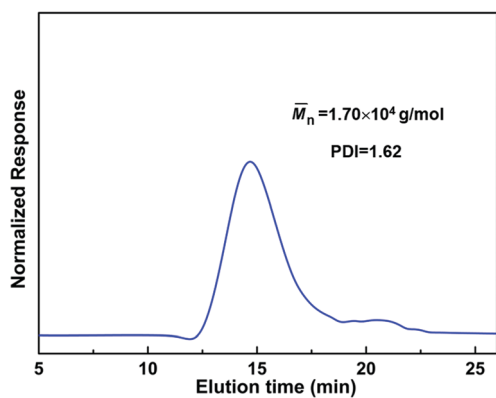


Fig. 2 GPC trace of PMP1 random copolymer.

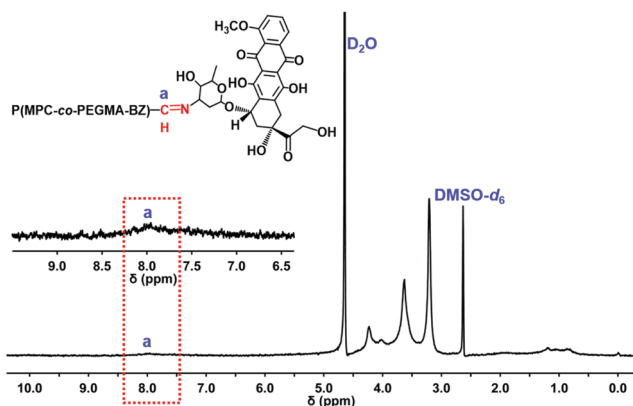


Fig. 3  $^1\text{H}$  NMR spectrum of PMPD1 prodrug.

$$\frac{A_{c'+d'+m}}{A_k} = \frac{32x + 9y}{2} \quad (2)$$

where  $A_k$ ,  $A_n$ , and  $A_{c'+d'+m}$  were the integral values of the peaks  $k$ ,  $n$ , and  $c' + d' + m$  in Fig. 1, respectively.

The  $\bar{M}_{n,\text{NMR}}$  of the P(MPC-*co*-PEGMA-BZ) random copolymer was calculated using the following eqn (3):

$$\bar{M}_{n,\text{NMR}} = 632x + 294.73y + 264.86 \quad (3)$$

where  $632 \text{ g mol}^{-1}$  and  $294.73 \text{ g mol}^{-1}$  were the molecular weights of one repeating unit of the PEGMA-BZ and MPC, respectively, and  $264.86 \text{ g mol}^{-1}$  was the molecular weight of the CEP.  $x$  and  $y$  represent the polymerization degrees of PEGMA-BZ and MPC, respectively.

The new peak at  $\delta$  8.01 ppm (peak a) can be attributed to the  $-\text{HC}=\text{N}-$  of the P(MPC-*co*-PEGMA-BZ)-*g*-DOX prodrug in Fig. 3, which demonstrates that the PMPD prodrug has been successfully prepared. The chemical structure of propargyl folate has been characterized by  $^1\text{H}$  NMR and is shown in Fig. S5 (ESI $^\dagger$ ). The thiol ( $-\text{SH}$ )-functionalized P(MPC-*co*-PEGMA-BZ)-*g*-DOX was obtained by an aminolysis reaction. We can confirm the successful synthesis of the thiol-functionalized prodrug due to the discernible UV-vis peaks of the  $-\text{SH}$  group, as seen in Fig. S6 (B, red line) (ESI $^\dagger$ ). Subsequently, the FA-P(MPC-*co*-PEGMA-BZ)-*g*-DOX prodrug was prepared by click chemistry method

Table 1 Size ( $\bar{D}_z$ ), size PDI, DOX content and FA content of PMPD1 and FA-PMPD1 prodrug nanoparticles

Sample	$\bar{D}_z^a$ (nm)	Size PDI $^a$	DOX content $^b$ (wt%)	FA content $^b$ (wt%)
PMPD-1	134	0.258	28.2	—
FA-PMPD-1	144	0.233	23.2	0.46

$^a$  Determined by DLS measurement.  $^b$  Determined by UV-vis measurement.

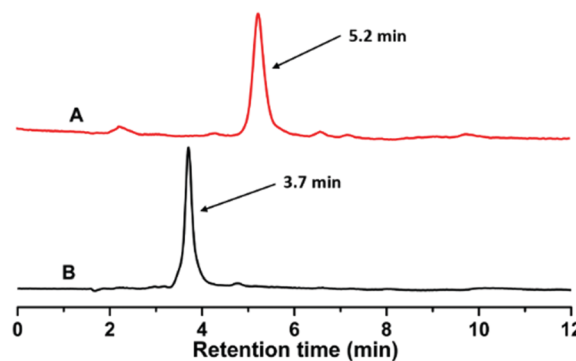


Fig. 4 HPLC analyses results of (A) free DOX and (B) PMPD1 prodrug. HPLC analyses were performed with acetonitrile/water (50 : 50, v/v), as the mobile phase at  $30^\circ\text{C}$  with a flow rate of  $1.0 \text{ mL min}^{-1}$ .

(abbreviated as FA-PMPD1). The UV-vis spectra of FA and FA-PMPD1 prodrugs are shown in Fig. S7 (ESI $^\dagger$ ), in which we can find that the peak at 275 nm and 500 nm could be attributed to the specific absorption wavelengths of DOX and folate moieties in the FA-PMPD1 prodrug, respectively, indicating that the DOX and folate moieties have been successfully conjugated onto the copolymer. In this study, the DOX contents of PMPD1 and FA-PMPD1 have been calculated by eqn (S1) (ESI $^\dagger$ ), the results are listed in Table 1. Moreover, the folate content of FA-PMPD1 prodrug was calculated to be 0.46 wt% by eqn (S2) in the ESI $^\dagger$ .

For further verifying that the free DOX had been conjugated to the side chains of P(MPC-*co*-PEGMA-BZ), HPLC was used; the HPLC results are shown in Fig. 4. We can see that the free DOX elutes at 5.2 min in Fig. 4(A), while the PMPD1 prodrug elutes at 3.7 min in Fig. 4(B). There are no traces at 5.2 min in Fig. 4(B), which could confirm that P(MPC-*co*-PEGMA-BZ)-*g*-DOX has been purified and does not contain free DOX.

### Self-assembly of the polymeric prodrugs

The critical aggregation concentration (CAC) represents the thermodynamic stability of the nanoparticles in an aqueous medium. When the concentration of the prodrug is higher than the CAC value, the PMPD1 and FA-PMPD1 prodrug can self-assemble into nanoparticles with DOX as the core and hydrophilic P(MPC-*co*-PEGMA-BZ) as the shell in an aqueous solution. The CAC value of PMPD1 and FA-PMPD1 prodrug nanoparticles was determined by the steady-state fluorescence probe method using pyrene as the probe. The CAC values of the PMPD1 and FA-PMPD1 prodrug nanoparticles are  $47.9 \text{ mg L}^{-1}$  and  $51.8 \text{ mg L}^{-1}$  as shown in Fig. S8(A and B) (ESI $^\dagger$ ), respectively. The morphologies of PMPD1 and FA-PMPD1 nanoparticles

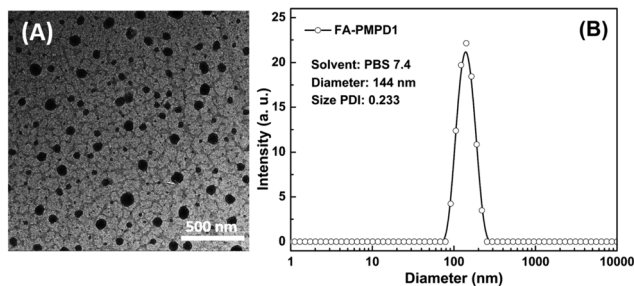


Fig. 5 TEM image of FA-PMPD1 prodrug nanoparticles (A) and the particle size distribution curve (B) corresponding to the TEM samples (scale bar 500 nm). The concentration was  $0.5 \text{ mg mL}^{-1}$ .

were observed by TEM analysis, while the average particle diameters ( $\bar{D}_z$ ) and size polydispersity index (size PDI) of the prodrug nanoparticles were determined by dynamic light scattering (DLS), and the results are listed in Table 1.

As illustrated in Fig. 5(A) and Fig. S9(A) (ESI<sup>†</sup>), the morphologies of PMPD1 and FA-PMPD1 prodrug nanoparticles exhibited relatively uniform distribution. For PMPD1 and FA-PMPD1 prodrug nanoparticles, the corresponding particle size distribution curves with an average diameter of 144 nm and 134 nm are displayed in Fig. 5(B) and Fig. S9(B) (ESI<sup>†</sup>), respectively.

The stability of FA-PMPD1 prodrug nanoparticles was then observed by DLS measurement. The prodrug nanoparticles could maintain good stability over a period of 50 days as shown in Fig. S10 (ESI<sup>†</sup>). The particle size distribution of FA-PMPD1 prodrug nanoparticles has almost no significant changes, which could be ascribed to the hydrophilic property of the zwitterionic PC moiety. These results indicate that the FA-PMPD1 prodrug nanoparticles with stealthy PC shell could prolong circulation time and have possibility to enhance tumor accumulation *in vivo*.<sup>56,57</sup>

### pH-Responsive ability and colloid stability of the prodrug nanoparticles

To investigate the pH-responsive ability of FA-PMPD1 prodrug nanoparticles, the particle size evolutions of FA-PMPD1 prodrug nanoparticles at pH 5.0 and 7.4 were determined by DLS measurement, respectively. As shown in Fig. 6, the size of the FA-PMPD1 prodrug nanoparticles showed no significant change at pH 7.4 for 48 h. However, the average size of the prodrug nanoparticles increased significantly with the increasing incubation time at pH 5.0. The size of the prodrug nanoparticles further expanded to hundreds of nanometers at 48 h intervals, or even larger. This may be caused by the aggregation of hydrophobic segments to form larger aggregates at pH 5.0 after 48 h, indicating that the FA-PMPD1 prodrug nanoparticles could be remarkably destroyed in an acidic medium.

In addition, we used TEM to observe the morphology changes in the FA-PMPD1 prodrug nanoparticles. As shown in Fig. 7(A), it should be noted that the morphology of the FA-PMPD1 prodrug nanoparticles could maintain the uniform structure under the condition of pH 7.4 at 48 h intervals. However, irregular aggregates were clearly observed at pH 5.0

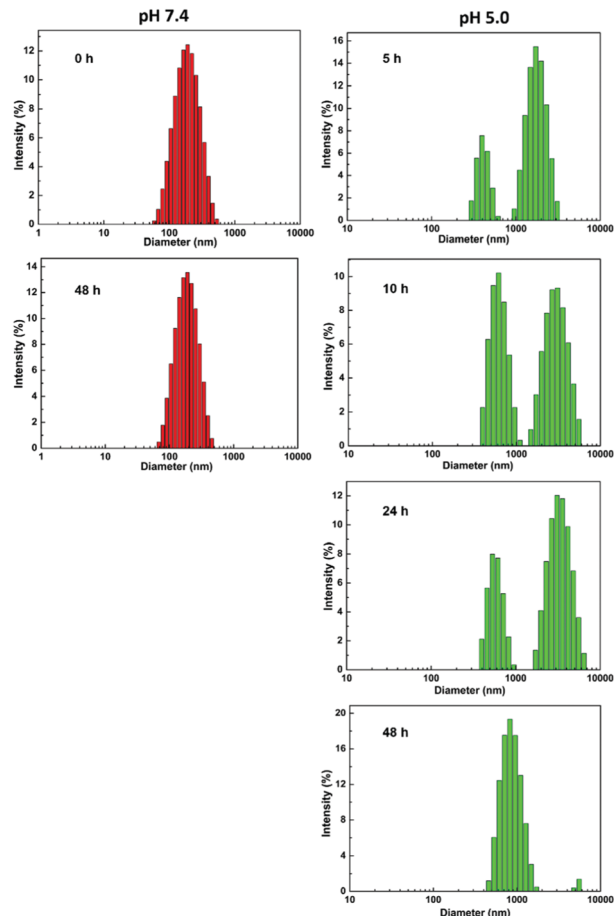


Fig. 6 Size change of FA-PMPD1 prodrug nanoparticles under different conditions of pH 7.4 and pH 5.0 as determined by DLS measurements.

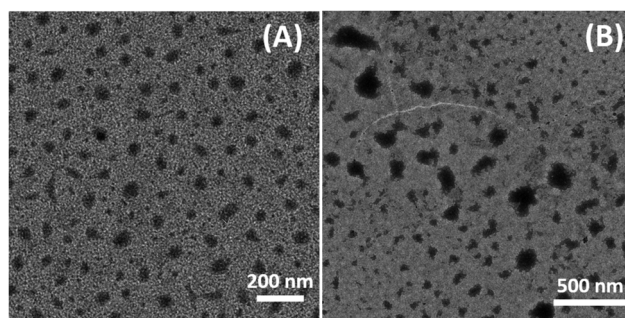


Fig. 7 TEM images of FA-PMPD1 prodrug nanoparticles incubation at pH 7.4 (A) and pH 5.0 (B) at 48 h intervals. The concentration of the prodrug nanoparticles was kept at  $0.5 \text{ mg mL}^{-1}$ .

after 48 h, as shown in Fig. 7(B). The results could indicate that FA-PMPD1 prodrug nanoparticles could maintain the stability under physiological conditions and the FA-PMPD1 prodrug nanoparticles could be dissociated under mildly acidic conditions. We can see that the results obtained from the DLS measurement in Fig. 6 are consistent with those of the TEM measurement in Fig. 7, indicating that the FA-PMPD1 prodrug nanoparticles have pH-responsive properties.

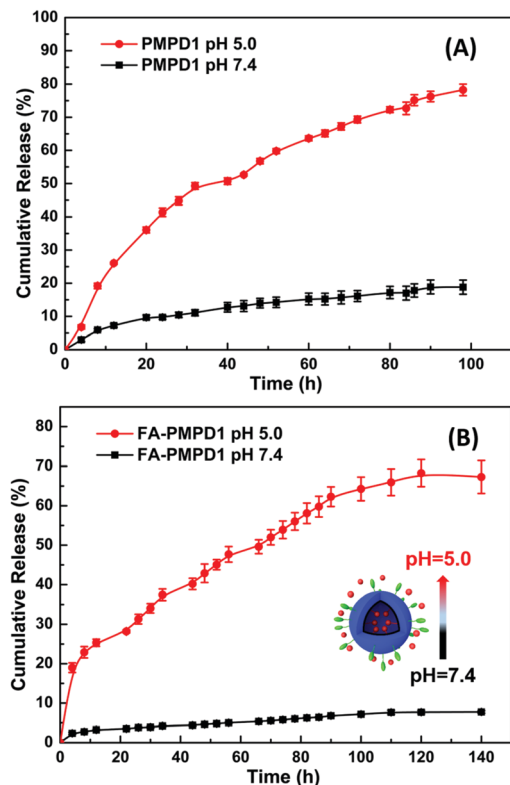


Fig. 8 *In vitro* DOX release curves for PMPD1 (A) and FA-PMPD1 (B) prodrug nanoparticles at pH 7.4 and pH 5.0. The nanoparticles concentration was  $1 \text{ mg mL}^{-1}$ .

***In vitro* drug release.** The release profiles of PMPD1 and FA-PMPD1 were studied at the physiological pH 7.4 and intracellular acidic pH 5.0. As shown in Fig. 8, approximately 80% of DOX was released from the PMPD1 prodrug nanoparticles after incubation for 98 h at pH 5.0, whereas the release of DOX was about 15% at pH 7.4. The DOX could be released from the FA-PMPD1 prodrug nanoparticles at pH 7.4, the final prodrug nanoparticles cumulative release rate was approximately 7.3% after 140 h. Notably, the DOX release was evidently accelerated at pH 5.0, and almost 70% of DOX was released from the FA-PMPD1 prodrug nanoparticles within 140 h, as shown in Fig. 8(B). These results indicate that the cleavage of the Schiff base bond and the disassembly of the prodrug nanoparticles could be accelerated at pH 5.0, which could indeed cause the fast release of DOX from the PMPD1 and FA-PMPD1 prodrug nanoparticles. In addition, the PMPD1 and FA-PMPD1 prodrug nanoparticles can reduce premature drug release in the bloodstream and promote drug burst release under endo/lysosomal acidic condition in the tumor cells.

***In vitro* cytotoxicity.** In this study, we used MTT assays to investigate the cytotoxicity of the PMP1 random copolymer against normal cells (L929 cells) and cancer cells (HeLa cells and HepG2 cells). In Fig. 9, the cell viability assays demonstrated that the PMP1 random copolymer has good biocompatibility and low toxicity against L929 cells. The same tendency was found in two other tumor cell lines, which could indicate that the PMP1 random copolymer may be a potential prospect as a

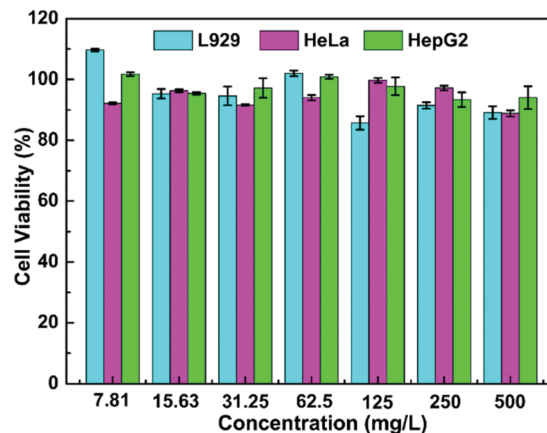


Fig. 9 Cell viabilities of L929 cells, HeLa cells, and HepG2 cells treated with PMP1 random copolymer at different concentrations with 48 h of incubation.

drug carrier to treat some ongoing challenges in current tumor treatment.

For evaluating their antitumor efficacy, the antiproliferation activities of the free DOX, PMPD1, and FA-PMPD1 prodrug nanoparticles against HeLa cells were investigated using MTT assays; this is because the folate receptor was over-expressed in the HeLa cells.<sup>45,58</sup> As shown in Fig. 10, the cell viabilities of HeLa cells decreased gradually when the DOX concentration increased from  $0.02 \text{ mg L}^{-1}$  to  $10 \text{ mg L}^{-1}$ . The half-maximal inhibitory concentration ( $IC_{50}$ ) values of free DOX, PMPD1, and FA-PMPD1 prodrug nanoparticles against HeLa cells were determined to be  $0.17 \text{ mg L}^{-1}$ ,  $0.76 \text{ mg L}^{-1}$ , and  $0.62 \text{ mg L}^{-1}$ , respectively. The *in vitro* antitumor efficacy of free DOX was higher than those of the PMPD1 and FA-PMPD1 prodrug nanoparticles because it is easily diffused through the cellular membrane, enhancing the antitumor function of free DOX.<sup>59–61</sup> Another reason is due to the overexpressed folate  $FR\alpha$  receptors in HeLa cells, which can indeed lead to enhanced cytotoxicity of the FA-PMPD1 prodrug nanoparticles. We further monitored the endocytosis process by a living cell-image system. The results

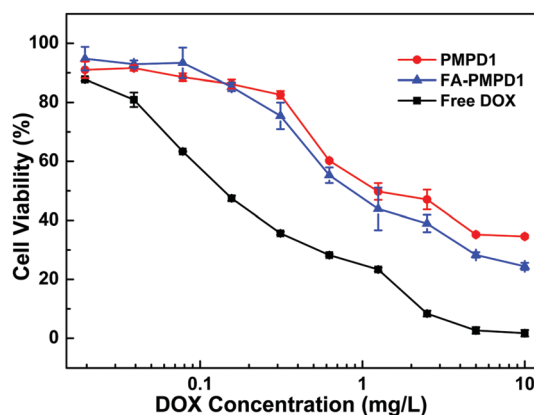


Fig. 10 Cell viability of HeLa cells treated with free DOX, PMPD1, and FA-PMPD1 with different DOX dosages for 48 h of incubation. The  $IC_{50}$  values of free DOX, PMPD1, and FA-PMPD1 were calculated by GraphPad Prism 5 software.

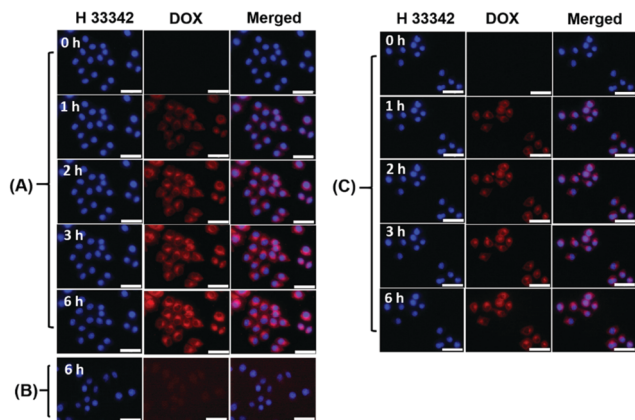


Fig. 11 Live cell-imaging system images of HeLa cells incubated with (A) FA-PMPD1 nanoparticles, (B) free DOX and (C) PMPD1 nanoparticles at different times. (The DOX dosage was  $4 \text{ mg L}^{-1}$ .) For each panel, images from left to right show cell nuclei stained by H 33342 (blue), DOX fluorescence in cells (red), and overlays of the blue and red images. The scale bars are  $50 \mu\text{m}$  in all images.

showed that FA-PMPD1 prodrug had better endocytosis effect (Fig. 11A) than those of free DOX (Fig. 11B) and the non-targeted PMPD1 prodrug nanoparticles (Fig. 11C) in HeLa cells,<sup>62,63</sup> demonstrating that the folate enhanced the targeting ability of the FA-PMPD1 prodrug nanoparticles on internalization of HeLa cells.

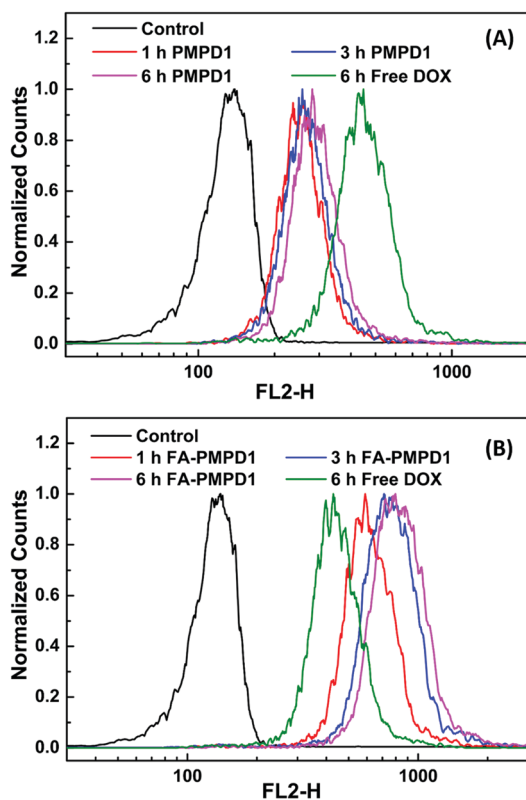


Fig. 12 Flow cytometry curves of HeLa cells treated with (A) PMPD1 and (B) FA-PMPD1 prodrug nanoparticles for different times (1 h, 3 h, and 6 h) with a certain concentration of DOX ( $4 \text{ mg L}^{-1}$ ).

For analysing the fluorescence intensity of HeLa cells incubated with free DOX, PMPD1, and FA-PMPD1 prodrug nanoparticles for fixed time intervals (1 h, 3 h, and 6 h), we recorded the fluorescence intensity of HeLa cells using flow cytometry. As shown in Fig. 12, the relative geometrical mean fluorescence intensities of the HeLa cells with PMPD1 and FA-PMPD1 prodrug nanoparticles increased with increasing time. Notably, there are stronger DOX fluorescence intensities at 6 h than at 1 h, indicating that the uptake of nanoparticles was a time-dependent property. We could find that the fluorescence intensity of the free DOX was higher than that of the PMPD1 prodrug nanoparticles incubated for 6 h, as shown in Fig. 12(A). FA-PMPD1 prodrug nanoparticles had significantly higher cellular uptake than free DOX at the same incubation time, as seen in Fig. 12(B), implying that FA could enhance the phagocytosis of FA-PMPD1 by the over-expression of FA receptors on the HeLa cells surface.

## Conclusions

In summary, we have developed a novel pH-sensitive zwitterionic prodrug FA-P(MPC-*co*-PEGMA-BZ)-*g*-DOX with a combination of RAFT and click chemistry methods. The zwitterionic polymeric prodrug could self-assemble into nanoparticles, which possesses good stability due to the stealthy phosphorylcholine (PC) and PEGMA moiety under physiological conditions. The covalently linked DOX could be released from the FA-PMPD prodrug nanoparticles due to the cleavage of the benzoic-imine bond at pH 5.0, and an accumulative DOX release of FA-PMPD1 prodrug nanoparticles was up to 70.0%, demonstrating a remarkable pH-triggered drug release behavior. In addition, the *in vitro* MTT assay results revealed that the PMPD and FA-PMPD prodrug nanoparticles could exhibit superior antitumor effects against HeLa cells with  $\text{IC}_{50}$  of  $0.76 \text{ mg L}^{-1}$  and  $0.62 \text{ mg L}^{-1}$  after 48 h of incubation, respectively. Meanwhile, we utilized cellular uptake and flow cytometry analyses to confirm that the FA-PMPD prodrug nanoparticles possessed targeting ability. This is due to the presence of large amount of over-expression FA receptors on HeLa cell surface. Therefore, the cell membrane mimicking zwitterionic FA-P(MPC-*co*-PEGMA-BZ)-*g*-DOX prodrug nanoparticles show great potential in the application of cancer treatment.

## Conflicts of interest

The authors declare no competing financial interest.

## Acknowledgements

We gratefully acknowledge the financial supports from the National Natural Science Foundation of China (21374066), the Major Program of the Natural Science Project of Jiangsu Higher Education Institutions (15KJA150007), the Natural Science Foundation of Jiangsu Province (BK20171212), a Project Funded by the Priority Academic Program Development (PAPD) of Jiangsu Higher Education Institutions, and Soochow-Waterloo

University Joint Project for Nanotechnology from Suzhou Industrial Park. Mr Lei Li would like to thank the financial support from the Innovative Graduate Research Program of Jiangsu Province (KYCX17\_1981).

## References

- X. S. Li, J. Kim, J. Yoon and X. Y. Chen, *Adv. Mater.*, 2017, **29**, 1606857.
- C. X. Zheng, Y. Zhao and Y. Liu, *Chin. J. Polym. Sci.*, 2018, **36**, 322–346.
- K. Jeong, C. S. Kang, Y. Kim, Y. D. Lee, I. C. Kwon and S. Kim, *Cancer Lett.*, 2016, **374**, 31–43.
- J. Liu, J. L. He, M. Z. Zhang, G. Q. Xu and P. H. Ni, *J. Mater. Chem. B*, 2018, **6**, 3262–3273.
- W. J. Zhang, C. Y. Hong and C. Y. Pan, *Biomacromolecules*, 2016, **17**, 2992–2999.
- F. W. Zhang, G. Z. Zhu, O. Jacobson, Y. Liu, K. Chen, G. C. Yu, Q. Q. Ni, J. Fan, Z. Yang, F. Xu, X. Fu, Z. Wang, Y. Ma, G. Niu, X. B. Zhao and X. Y. Chen, *ACS Nano*, 2017, **11**, 8838–8848.
- Y. Z. Men, S. J. Peng, P. Yang, Q. Jiang, Y. H. Zhang, B. Shen, P. Dong, Z. Q. Pang and W. L. Yang, *ACS Appl. Mater. Interfaces*, 2018, **10**, 23509–23521.
- J. B. Schlenoff, *Langmuir*, 2014, **30**, 9625–9636.
- Q. Shao and S. Y. Jiang, *Adv. Mater.*, 2015, **27**, 15–26.
- G. J. Hu and T. Emrick, *J. Am. Chem. Soc.*, 2016, **138**, 1828–1831.
- B. L. Prity, C. Elisha, C. Peggy and A. Ayse, *ACS Appl. Mater. Interfaces*, 2017, **9**, 20859–20872.
- X. F. Yu, Z. H. Liu, J. Janzen, I. Chafeeva, S. Horte, W. Chen, R. K. Kainthan, J. N. Kizhakkedathu and D. E. Brooks, *Nat. Mater.*, 2012, **11**, 468–476.
- S. Li, Y. Y. Cai, J. Cao, M. T. Cai, Y. W. Chen and X. L. Luo, *Polym. Chem.*, 2017, **8**, 2472–2483.
- C. M. Xing, F. N. Meng, M. Quan, K. Ding, Y. Dang and Y. K. Gong, *Acta Biomater.*, 2017, **59**, 129–138.
- X. Y. Chen, T. C. Chen, Z. F. Lin, X. E. Li, W. Wu and J. S. Li, *Chem. Commun.*, 2015, **51**, 487–490.
- X. Q. Yang, N. Li, I. Constantinesco, K. Yu, J. N. Kizhakkedathu and D. E. Brooks, *Acta Biomater.*, 2016, **40**, 212–225.
- Y. N. Chou, A. Venault, Y. H. Wang, A. Chinnathambi, A. Higuchi and Y. Chang, *J. Mater. Chem. B*, 2018, **6**, 4909–4919.
- Y. Li, R. Y. Liu, Y. J. Shi, Z. Z. Zhang and X. Zhang, *Theranostics*, 2015, **5**, 583–596.
- X. Li, B. Wu, H. Chen, K. H. Nan, Y. Y. Jin, L. Sun and B. L. Wang, *J. Mater. Chem. B*, 2018, **6**, 4274–4292.
- X. J. Lin, K. Fukazawa and K. Ishihara, *ACS Appl. Mater. Interfaces*, 2015, **7**, 17489–17498.
- X. J. Chen, S. S. Parekar, E. Henchey, S. Schneider and T. Emrick, *Bioconjugate Chem.*, 2012, **23**, 1753–1763.
- Y. J. Chen, H. J. Han, H. X. Tong, T. T. Chen, H. B. Wang, J. Ji and Q. Jin, *ACS Appl. Mater. Interfaces*, 2016, **8**, 21185–21192.
- M. M. Zong and Y. K. Gong, *Chin. J. Polym. Sci.*, 2011, **29**, 53–64.
- Y. Iwasaki and K. Ishihara, *Sci. Technol. Adv. Mater.*, 2012, **13**, 064101.
- L. Ye, Y. B. Zhang, B. G. Yang, X. Zhou, J. J. Li, Z. H. Qin, D. Y. Dong, Y. L. Cui and F. L. Yao, *ACS Appl. Mater. Interfaces*, 2016, **8**, 4385–4398.
- X. P. Zhang, W. Chen, X. Y. Zhu and Y. F. Lu, *ACS Appl. Mater. Interfaces*, 2017, **9**, 7972–7978.
- Y. T. Wen, Z. X. Zhang and J. Li, *Adv. Funct. Mater.*, 2014, **24**, 3874–3884.
- Y. Ohara, K. Nakai, S. Ahmed, K. Matsumura, K. Ishihara and S. I. Yusa, *Langmuir*, 2018, DOI: 10.1021/acs.langmuir.8b00632.
- H. B. Wang, F. M. Xu, D. D. Li, X. S. Liu, Q. Jin and J. Ji, *Polym. Chem.*, 2013, **4**, 2004–2010.
- W. L. Wang, B. Wang, X. J. Ma, S. R. Liu, X. D. Shang and X. F. Yu, *Biomacromolecules*, 2016, **17**, 2223–2232.
- J. Zhao, Y. D. Chai, J. Zhang, P. F. Huang, K. Nakashima and Y. K. Gong, *Acta Biomater.*, 2015, **16**, 94–102.
- B. X. Ma, W. H. Zhuang, Y. N. Wang, R. F. Luo and Y. B. Wang, *Acta Biomater.*, 2018, **70**, 186–196.
- F. Li, J. L. He, M. Z. Zhang and P. H. Ni, *Polym. Chem.*, 2015, **6**, 5009–5014.
- M. H. Lee, E. J. Kim, H. Lee, S. Y. Park, K. S. Hong, J. S. Kim and J. L. Sessler, *Chem. Commun.*, 2016, **52**, 10551–10554.
- Y. D. Gu, Y. N. Zhong, F. H. Meng, R. Cheng, C. Deng and Z. Y. Zhong, *Biomacromolecules*, 2013, **14**, 2772–2780.
- Y. Y. Zhang, C. Teh, M. H. Li, C. Y. Ang, S. Y. Tan, Q. Y. Qu, V. Korzh and Y. L. Zhao, *Chem. Mater.*, 2016, **28**, 7039–7050.
- L. Qiu, C. R. Xu, F. Zhong, C. Y. Hong and C. Y. Pan, *ACS Appl. Mater. Interfaces*, 2016, **8**, 18347–18359.
- J. Mao, Y. Li, T. Wu, C. H. Yuan, B. R. Zeng, Y. T. Xu and L. Z. Dai, *ACS Appl. Mater. Interfaces*, 2016, **8**, 17109–17117.
- Y. L. Bao, M. X. Yin, X. M. Hu, X. T. Zhuang, Y. Sun, Y. Y. Guo, S. W. Tan and Z. P. Zhang, *J. Controlled Release*, 2016, **235**, 182–194.
- C. Gao, F. Tang, G. Y. Gong, J. Zhang, M. P. M. Hoi, S. M. Y. Lee and R. B. Wang, *Nanoscale*, 2017, **9**, 12533–12542.
- D. Li, J. D. Han, J. X. Ding, L. Chen and X. S. Chen, *Carbohydr. Polym.*, 2017, **161**, 33–41.
- Y. Yu, C. K. Chen, W. C. Law, E. Weinheimer, S. Sengupta, P. N. Prasad and C. Cheng, *Biomacromolecules*, 2014, **15**, 524–532.
- K. Hida, N. Maishi, Y. Sakurai, Y. Hida and H. Harashima, *Adv. Drug Delivery Rev.*, 2016, **99**, 140–147.
- N. J. Song, M. M. Ding, Z. C. Pan, J. H. Li, L. J. Zhou, H. Tan and Q. Fu, *Biomacromolecules*, 2013, **14**, 4407–4419.
- Y. W. Cao, J. L. He, J. Liu, M. Z. Zhang and P. H. Ni, *ACS Appl. Mater. Interfaces*, 2018, **10**, 7811–7820.
- N. Muhammad, N. Sadia, C. C. Zhu, C. Luo, Z. J. Guo and X. Y. Wang, *Chem. Commun.*, 2017, **53**, 9971–9974.
- Y. Singh, K. K. D. R. Viswanadham, A. K. Jajoriya, J. G. Meher, K. Raval, S. Jaiswal, J. Dewangan, H. K. Bora, S. K. Rath, J. Lal, D. P. Mishra and M. K. Chourasia, *Mol. Pharmaceutics*, 2017, **14**, 2749–2765.
- W. X. Luo, G. Wen, L. Yang, J. Tang, J. G. Wang, J. H. Wang, S. Y. Zhang, L. Zhang, F. Ma, L. L. Xiao, Y. Wang and Y. J. Li, *Theranostics*, 2017, **7**, 452–465.
- J. H. Seo, S. Kakinoki, Y. Inoue, T. Yamaoka, K. Ishihara and N. Yui, *J. Am. Chem. Soc.*, 2013, **135**, 5513–5516.

- 50 L. Y. Xu, Q. M. Bai, X. Zhang and H. Yang, *J. Controlled Release*, 2017, **252**, 73–82.
- 51 Y. Chen, W. B. Cao, J. L. Zhou, B. Pidhatika, B. Xiong, L. Huang, Q. Tian, Y. W. Shu, W. J. Wen, I. M. Hsing and H. K. Wu, *ACS Appl. Mater. Interfaces*, 2015, **7**, 2919–2930.
- 52 A. Wicki, D. Witzigmann, V. Balasubramanian and J. Huwyler, *J. Controlled Release*, 2015, **200**, 138–157.
- 53 D. W. Zhu, W. Tao, H. L. Zhang, G. Liu, T. Wang, L. H. Zhang, X. W. Zeng and L. Mei, *Acta Biomater.*, 2016, **30**, 144–154.
- 54 Z. Q. Lei, P. Xie, M. Z. Rong and M. Q. Zhang, *J. Mater. Chem. A*, 2015, **3**, 19662–19668.
- 55 P. De, S. R. Gondi and B. S. Sumerlin, *Biomacromolecules*, 2008, **9**, 1064–1070.
- 56 W. L. Wang, B. Wang, S. R. Liu, X. D. Shang, X. X. Yan, Z. H. Liu, X. J. Ma and X. F. Yu, *ACS Appl. Mater. Interfaces*, 2017, **9**, 15986–15994.
- 57 P. S. Huang, H. J. Song, W. W. Wang, Y. Sun, J. H. Zhou, X. Wang, J. J. Liu, J. F. Liu, D. L. Kong and A. J. Dong, *Biomacromolecules*, 2014, **15**, 3128–3138.
- 58 D. Q. Chen, P. Song, F. Jiang, X. Y. Meng, W. P. Sui, C. Y. Shu and L. J. Wan, *J. Phys. Chem. B*, 2013, **117**, 1261–1268.
- 59 S. V. Lale, A. Kumar, S. Prasad, A. C. Bharti and V. Koul, *Biomacromolecules*, 2015, **16**, 1736–1752.
- 60 Y. Wang, Q. J. Luo, W. P. Zhu, X. D. Li and Z. Q. Shen, *Polym. Chem.*, 2016, **7**, 2665–2673.
- 61 H. R. Wang, J. L. He, D. L. Cao, M. Z. Zhang, F. Li, K. C. Tam and P. H. Ni, *Polym. Chem.*, 2015, **6**, 4809–4818.
- 62 Y. M. Zhang, F. Huang, C. H. Ren, L. J. Yang, J. F. Liu, Z. Cheng, L. P. Chu and J. J. Liu, *ACS Appl. Mater. Interfaces*, 2017, **9**, 13016–13028.
- 63 X. Q. Yang, J. J. Grailer, I. J. Rowland, A. Javadi, S. A. Hurley, V. Z. Matson, D. A. Steeber and S. Q. Gong, *ACS Nano*, 2010, **4**, 6805–6817.